EPJ Web of Conferences **23**, 00005 (2012)
DOI: 10.1051/epjconf/20122300005

Identification of Nodal Kink in Electron-Doped $(Nd_{1.85}Ce_{0.15})CuO_4$ Superconductor from Laser-Based Angle-Resolved Photoemission Spectroscopy

Haiyun Liu[1], Guodong Liu[1], Wentao Zhang[1], Lin Zhao[1], Jianqiao Meng[1], Xiaowen Jia[1], Xiaoli Dong[1], Wei Lu[1], Guiling Wang[2], Yong Zhou[2], Yong Zhu[3], Xiaoyang Wang[3], Tao Wu[4], Xianhui Chen[4], T. Sasagawa[5], Zuyan Xu[2], Chuangtian Chen[3] and X. J. Zhou[1,a]

[1] National Laboratory for Superconductivity, Beijing National Laboratory for Condensed Matter Physics, Institute of Physics, Chinese Academy of Sciences, Beijing 100190, China
[2] Laboratory for Optics, Beijing National Laboratory for Condensed Matter Physics,Institute of Physics, Chinese Academy of Sciences, Beijing 100190, China
[3] Technical Institute of Physics and Chemistry, Chinese Academy of Sciences, Beijing 100190, China
[4] Department of Physics, University of Science and Technology of China, Anhui, China
[5] Materials and Structures Laboratory, Tokyo Institute of Technology, Yokohama Kanagawa, Japan

Abstract. High-resolution laser-based angle-resolved photoemission measurements have been carried out on the electron-doped $(Nd_{1.85}Ce_{0.15})CuO_4$ high temperature superconductor. We have revealed a clear kink at ~60 meV in the dispersion along the (0,0)-(π,π) nodal direction, accompanied by a peak-dip-hump feature in the photoemission spectra. This indicates that the nodal electrons are coupled to collective excitations (bosons) in electron-doped superconductors, with the phonons as the most likely candidate of the boson. This finding has established a universality of nodal electron coupling in both hole- and electron-doped high temperature cuprate superconductors.

High temperature superconductivity in cuprates is achieved by doping an appropriate amount of charge carriers (electrons or holes) into the parent antiferromagnetic Mott insulators[1]. It is known that the unusual physical properties of high-T_c cuprate superconductors stem from the complex interplay between electron charge, spin and lattice vibrations. Investigation of these many-body effects is essential to understand the macroscopic physical properties and the mechanism of high temperature superconductivity. High resolution angle-resolved photoemission spectroscopy (ARPES) has become a powerful tool to probe many-body effects because the interaction of electrons with a collective excitation gives rise to a change in the electron self-energy which can be measured directly from ARPES[2]. In hole-doped cuprates, ARPES measurements have revealed a ubiquitous existence of a kink in the dispersion at ~70meV along the (0,0)-(π,π) nodal direction signaling an electron coupling with low energy collective excitations (phonons or magnetic resonance mode)[3–8]. In the electron-doped cuprates, indication of the nodal kink was found recently[9] which was not identified before[10–12]. It is well-known that the electron-doped superconductors exhibit different behaviors from its hole-doped counterparts, such as the narrower superconducting doping range and lower superconducting transition temperature (T_c)[13]. This raises interesting questions on whether the nodal electron dynamics in the electron-doped cuprates is inherently different from the hole-doped ones and whether such a difference may be responsible for the distinct behaviors between the electron- and hole-doped cuprates[14].

In this paper we report an identification of a kink in the nodal dispersion of the electron-doped $(Nd_{1.85}Ce_{0.15})CuO_4$ superconductor by taking advantage of the high performance laser-based ARPES system. In both optimally-doped and underdoped $(Nd_{1.85}Ce_{0.15})CuO_4$ superconductors, we have clearly identified a kink in the nodal dispersion near 60 meV, accompanied by peak-dip-hump structure in the photoemission spectra and a drop in the quasiparticle scattering rate. These observations indicate that, in the electron-doped cuprates, the nodal electrons couple with some collective excitations with phonons as the most likely candidate. It has established a universality of the nodal kink in both electron- and hole-doped cuprate superconductors. It also suggests that the different behaviors between electron- and hole-doped cuprates may not be dictated by the nodal electron coupling, but by their distinct doping-dependent electronic structure.

The angle-resolved photoemission measurements were performed on our recently developed vacuum ultra-violet (VUV) laser-based ARPES system at the Institute of Physics, Chinese Academy of Sciences, which has some unique advantages such as super-high energy resolution (better than 1 meV), high momentum resolution, super-high photon flux and enhanced bulk sensitivity[15]. The photon energy of the VUV laser is 6.994 eV with a bandwidth of 0.26 meV. Because of the relatively weaker photoemission cross section of the electron-doped $(Nd_{1.85}Ce_{0.15})CuO_4$ samples, the energy resolution of the electron energy analyzer (Scienta R4000) was set at 6.25 meV, giving rise to an overall en-

[a] Corresponding author: XJZhou@aphy.iphy.ac.cn

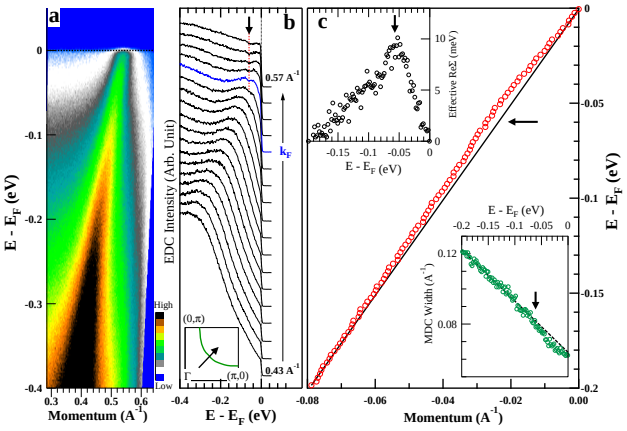

Fig. 1. Nodal kink in the optimally-doped $(Nd_{0.85}Ce_{0.15})CuO4$ (T_c=24 K) sample. (a). Photoemission image along the (0,0)-(π,π) nodal direction at 13 K. The location of the momentum cut is shown in the inset of (b). (b). The corresponding photoemission spectra. The EDCs near the Fermi momentum shows a peak-dip-hump structure, with the dip position marked by a dashed red line. (c). Nodal dispersion extracted from the MDC analysis. The black straight line is a guide to the eye which also serves as an empirical bare band to extract the effective real part of electron self-energy (ReΣ), as shown in the upper-left inset. The bottom-right inset shows the MDC width. The black dashed line is a guide to the eye.

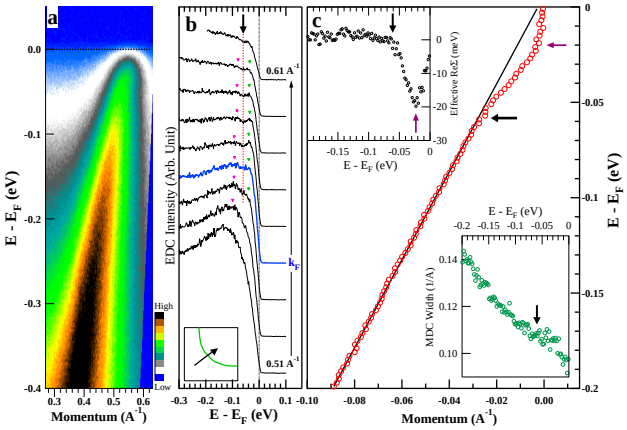

Fig. 2. Nodal kink in the slightly underdoped $(Nd_{0.85}Ce_{0.15})CuO4$ (T_c=20 K) sample. (a). Photoemission image along the (0,0)-(π,π) nodal direction at 15 K. The location of the momentum cut is shown in the inset of (b). (b). The corresponding photoemission spectra. The EDCs near the Fermi momentum shows a peak-dip-hump structure, with the peak and hump positions marked by triangles and the dip position marked by a dashed red line. (c). Nodal dispersion extracted from the MDC analysis. The black straight line is a guide to the eye which also serves as an empirical bare band to extract the effective real part of electron self-energy (ReΣ), as shown in the upper-left inset. A kink in the dispersion as well as an abrupt change in the effective ReΣ can be identified at ~60 meV, as indicated by black arrows. Another kink near 23 meV can also be seen in the dispersion and the effective ReΣ, as indicated by the purple arrows. The bottom-right inset shows the MDC width.

ergy resolution of 6.26 meV. The angular resolution is ~0.3°, corresponding to a momentum resolution ~0.004 $Å^{-1}$ at the photon energy of 6.994 eV. The Fermi level is determined by referencing to the Fermi edge of a clean polycrystalline gold that is electrically connected to the sample. The $(Nd_{1.85}Ce_{0.15})CuO_{4+\delta}$ single crystals were grown by flux method[16] or floating zone furnace. By annealing the as-grown single crystals in argon atmosphere to control the oxygen content, δ, we obtained two kinds of superconducting samples, one is close to optimally-doped with a T_c=24 K while the other is slightly underdoped with a T_c=20 K. The single crystals were cleaved *in situ* and measured in ultra-high vacuum with a base pressure better than 5×10^{-11} Torr.

Fig. 1 shows the photoemission data of the optimally-doped $(Nd_{0.85}Ce_{0.15})CuO4$ (T_c=24 K) sample measured along the (0,0)-(π,π) nodal direction at a temperature of 13 K. A clear band dispersion is observed in the raw data (Fig. 1a). By fitting the corresponding MDCs (momentum distribution curves), the quantitative dispersion is obtained as plotted in Fig. 1c. A weak but clear kink is present in the dispersion at an energy of ~60 meV, as indicated by the arrow in Fig. 1c. By choosing the straight line connecting the two points in the dispersion at E_F and -0.2 eV as an empirical bare band, the corresponding "effective real part of electron self-energy (ReΣ)" is extracted (up-left inset of Fig. 1c) with the ~60 meV feature showing up more clearly. In the corresponding MDC width (bottom-right inset of Fig. 1c), which is related to the quasiparticle scattering rate or the imaginary part of the electron self-energy, a slight drop is discernable near ~60 meV, as seen in the deviation of the MDC width data from a linear line. In the corresponding photoemission spectra (energy distribution curves, EDCs) as shown in Fig. 1b, the EDCs near the Fermi momentum show clear double-peak or peak-dip-hump structure, with a location of the dip at ~60 meV, as indicated by the dashed red line in Fig. 1b.

The photoemission data for the slightly underdoped $(Nd_{0.85}Ce_{0.15})CuO4$ (T_c=20 K) sample (Fig. 2) show some similar features as those in the optimally-doped sample (Fig. 1). First, a clear kink near ~60 meV is present in the MDC-derived dispersion (Fig. 2c) and more clearly in the corresponding effective real part of the electron self-energy (up-left inset of Fig. 2c). Second, in the corresponding EDCs near the Fermi momentum (Fig. 2b), the peak-dip-hump structure can be seen with a dip energy at ~60 meV. Here because of the data scattering it is hard to discern a clear feature in the MDC width (bottom-right inset of Fig. 2c) . An obvious difference in the data for the slightly underdoped sample is the observation of another kink at lower binding energy, ~23 meV, as seen in the dispersion (Fig. 2c) and the corresponding effective real part of electron self-energy (up-left inset of Fig. 2c). This ~23 meV kink arises because of the existence of a gap along the nodal direction. This gap opening is evidenced by the corresponding peak position of the EDC at the Fermi momentum which is about 35 meV below the Fermi level (the corresponding EDC leading edge is about 12 meV below the Fermi level) (Fig. 2b). The appearance of the low energy kink and nearly vertical dispersion is similar to that found in the hole-doped superconductors when a superconducting gap opens below T_c[17]. Note that this nodal gap in the underdoped $(Nd_{0.85}Ce_{0.15})CuO4$ (T_c=20 K) sample is a band gap, but not the superconducting gap which is zero along the nodal direction[10, 18, 19].

Fig. 3 shows momentum dependence of the ~60 meV kink feature in dispersions for the $(Nd_{0.85}Ce_{0.15})CuO4$ samples. For the optimally-doped sample (T_c=24 K) (Fig. 3a), the ~60 meV kink persists over a relatively large momentum space that is covered, with the kink feature getting slightly weaker when the momentum move away from the nodal region (Fig. 3a). Also note in this momentum space, there is no indication of band gap opening, as seen from the EDCs on the Fermi surface(Fig. 3b). For the slightly underdoped sample (T_c=20 K) (Fig. 3c), a band gap is present near the nodal region which gets larger when the momentum moves away from the nodal region, as seen from the position of EDCs on the Fermi surface (Fig. 3d). This observation is consistent with the previous measurements[20,21]. The gap size increase shifts the energy position upwards for the kink induced by the band gap (Fig. 3c). As shown in Fig. 3c, for the momentum cuts closest to the nodal direction (Cuts 1 and 2), there is a clear ~60 meV kink in dispersions with the band-gap-induced kink confined to a low energy (~23 meV). For the Cut 3, even though the band-gap-induced kink energy gets higher (~34 meV) one can still observe the ~60 meV kink which appears to get weaker than that for Cuts 1 and 2. For the Cut 4, the band-gap-induced kink has a comparable energy scale at ~60 meV, making the ~60 meV kink hard to observe.

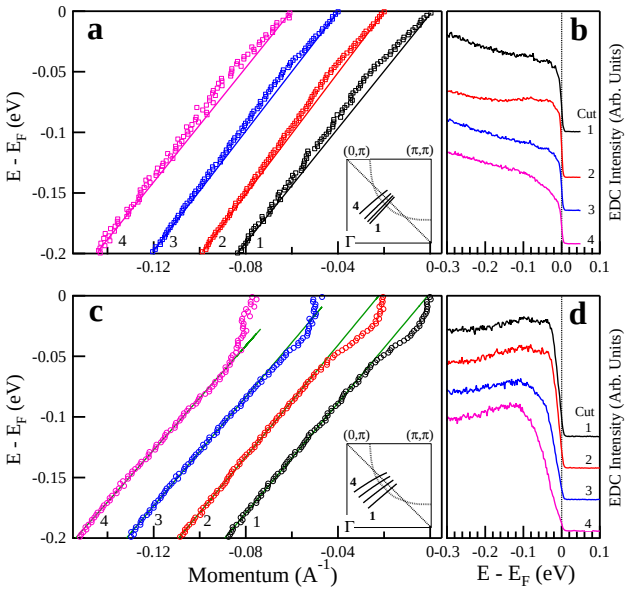

Fig. 3. Momentum dependence of the dispersion and photoemission spectra on the Fermi surface in $(Nd_{1.85}Ce_{0.15})CuO_4$ superconductors. (a). Momentum-dependent dispersions for the optimally-doped $(Nd_{1.85}Ce_{0.15})CuO_4$ (T_c=24 K) sample. The solid lines are guides to the eye. The location of the momentum cuts are marked in the bottom-right inset. For clarity, dispersions are offset along the momentum axis. (b). EDCs on the Fermi surface for the $(Nd_{1.85}Ce_{0.15})CuO_4$ (T_c=24 K) sample. (c). Momentum-dependent dispersions for the slightly underdoped $(Nd_{1.85}Ce_{0.15})CuO_4$ (T_c=20 K) sample. The solid lines are guides to the eye. The location of the momentum cuts are marked in the bottom-right inset. For clarity, dispersions are offset along the momentum axis. (d). EDCs on the Fermi surface for the $(Nd_{1.85}Ce_{0.15})CuO_4$ (T_c=20 K) sample.

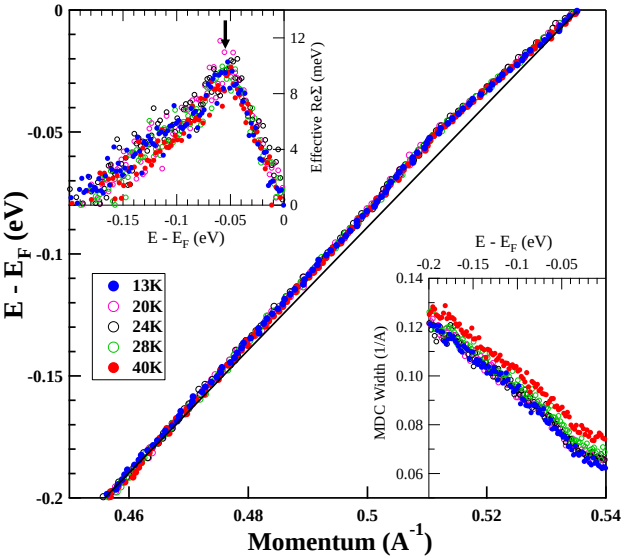

Fig. 4. Temperature dependence of the nodal dispersion in the optimlly-doped $(Nd_{1.85}Ce_{0.15})CuO_4$ (T_c=24 K) sample. The black line is a guide to the eye which also serves as an empirical bare band to extract the effective real part of electron self-energy, $Re\Sigma$, as shown in the upper-left inset. The bottom-right inset shows the MDC width measured at various temperatures.

Fig. 4 shows the temperature dependence of the ~60 meV nodal kink in the optimally-doped $(Nd_{0.85}Ce_{0.15})CuO4$ (T_c=24 K) sample. It is clear that the ~60 meV kink is present over the entire temperature range measured: both below T_c and above T_c. Particularly, there is little change observed across the superconducting transition temperature.

The above systematic measurements on the doping-, momentum- and temperature-dependence of the nodal ~60 meV kink provide important information to judge on its origin in the electron-doped $(Nd_{1.85}Ce_{0.15})CuO_4$ superconductors. We note that, before the nodal kink was identified in the electron-doped superconductors[9], there were reports on the signatures of a kink near the (π, 0) antinodal region[10–12]. Such an antinodal kink is attributed either to the band-folding effect or to the mode coupling[10–12]. In the electron-doped cuprates, the commensurate antiferromagnetic fluctuation is found to be strong and may coexist with superconductivity[22], which may give rise to a band folding with respect to the antiferromagnetic zone boundary. In this case, the original band and the folded band cross, forming a gap at the intersection, and separate into two (upper and lower) band sections[12]. Such a picture was proposed to account for the kink and the peak-dip-hump structure near the antinodal region[12]. However, this scenario is not applicable to the kink we have observed near the nodal region. In terms of the band-folding picture, because the upper section of the band is well above the Fermi energy along the nodal direction, the band folding effect on the occupied state is expected to be minimal[12]. Particularly, it would not produce the peak-dip-hump structure as we have observed in EDCs near the nodal region (Figs. 1b and 2b).

The above observations of the nodal ~60 meV kink in the dispersion, a drop in the quasiparticle scattering rate and the peak-dip-hump structure in EDCs in the electron-

doped superconductors show a clear resemblance to those found in the hole-doped counterparts[3–8]. These strongly suggest that the nodal ~60 meV kink in the electron-doped cuprates is due to the electron coupling with some collective excitations (bosons). Concerning the nature of the involved boson(s), the available candidates that are present in the electron-doped cuprates are either magnetic resonance mode[23] or phonons. The possibility of the magnetic resonance mode can be easily ruled out because its energy scale (~10 meV)[23] is far off from 60 meV. This has left phonons as the most viable candidate with its comparable energy scale. The temperature dependence measurement (Fig. 4) lends further support to the phonon scenario. In the electron-doped cuprates, the oxygen vibrations in the CuO_2 planes produce phonon modes in the energy range of 50~80 meV[24–26]. Particularly, the mode with the bond-stretching character has an energy near 60 meV and exhibits an anomalous softening indicative of strong electron-phonon coupling[26]. This makes the electron coupling with this particular phonon mode the most likely case for the nodal ~60 meV energy scale in the electron-doped cuprates.

Our present work has clearly established the nodal kink as a universal feature for both the electron-doped and hole-doped cuprates. Although the mode coupling strength[27] of the electron-doped superconductors (λ~0.20 for the optimally-doped $(Nd_{1.85}Ce_{0.15})CuO_4$) is weaker than that in the hole-doped counterparts (λ~0.55 for the optimally-doped $(La_{1.85}Sr_{0.15})CuO_4$[7]), such a quantitative difference may not account for the dramatically different behaviors between the electron- and hole-doped cuprates[13]. One most notable distinction between the electron- and hole-doped cuprates is the different doping evolution of the electronic structure. In the hole-doped cuprates, upon doping the antiferromagnetic parent compound, the low-lying states first develop near the nodal region while the antinodal region is gapped at low dopings[28–30]. In the electron-doped case, by contrast, the antinodal state first develops upon doping[31] while the nodal region is gapped at low dopings (Figs. 2 and 3d). Such a dichotomy in the electronic structure may play more important role in dictating the different behaviors between the electron-doped and hole-doped cuprates.

In summary, by taking high quality data from the laser-based ARPES, we have clearly identified a nodal kink at ~60 meV in the electron-doped cuprate superconductors. This has established a universality of the 60 meV nodal kink in both electron- and hole-doped high temperature superconductors. The origin of the ~60 meV kink is attributed to the electron coupling with some collective excitations, with the phonons being the most likely candidate. This finding also suggests that the nodal electron coupling may not be the major player for understanding different behaviors between the electron- and hole-doped cuprates.

This work is supported by the NSFC (Grant No. 10734120) and the MOST of China (973 program No: 2011CB921703).

References

1. P. A. Lee, N. Nagaosa and X.-G. Wen, Rev. Mod. Phys. **78**, 17 (2006).
2. A. Damascelli et al., Rev. Mod. Phys. **75**, 473(2003); J. C. Campuzano et al., in The Physics of Superconductors, Vol. 2, edited by K. H. Bennemann and J. B. Ketterson, (Springer, 2004); X. J. Zhou et al., in Handbook of High Temperature Superconductivity: Theory and Experiment, edited by J. R. Schrieffer, (Springer, 2007).
3. P. V. Bogdanov et al., Phys. Rev. Lett. **85**, 2581 (2000).
4. P. Johnson et al., Phys. Rev. Lett. **87**, 177007 (2001).
5. A. Kaminski et al., Phys. Rev. Lett. **86**, 1070 (2001).
6. A. Lanzara et al., Nature (London) **412**, 510 (2001).
7. X. J. Zhou et al., Nature (London) **423**, 398 (2003).
8. A. A. Kordyuk et al., Phys. Rev. Lett. **97**, 017002 (2006).
9. F. Schmitt et al., arXiv:cond-mat/0808.0476, Phys. Rev. B **78**, 100505 (2008); S. R. Park et al., arXiv:cond-mat/0808.0559, Phys. Rev. Lett. **101**, 117006 (2008); H. Y. Liu et al., arXiv:cond-mat:0808.0802.
10. T. Sato et al., Science **291**, 1517 (2001).
11. N. P. Armitage et al., Phys. Rev. B **68**, 064517 (2003).
12. H. Matsui et al., Phys. Rev. Lett. **95**, 017003 (2005).
13. Y. Tokura et al., Nature (London) **337**, 345 (1989).
14. Z. -X. Shen, A. Lanzara, S. Ishihara, and N. Nagaosa, Philos. Mag. B **82**, 1349 (2002).
15. G. D Liu et al., Rev. Sci. Instrument. **79**, 023105 (2008).
16. X. H. Chen et al., Phys. Rev. B **72**, 064517 (2005).
17. M. Norman et al., Phys. Rev. B **64**, 184508 (2001).
18. N.P Armitage et al., Phys. Rev. Lett. **86**, 1126(2001).
19. H. Matsui et al., Phys. Rev. Lett. **94**, 047005 (2005).
20. N. P. Armitage et al., Phys. Rev. Lett. **88**, 257001 (2002).
21. H. Matsui et al., Phys. Rev. B **75**, 224514 (2007).
22. K. Yamada et al., Phys. Rev. Lett. **90**, 137004 (2003).
23. J. Zhao et al., Phys. Rev. Lett **99**, 017001 (2007).
24. H. J. Kang et al., Phys. Rev. B **66**, 064506 (2002).
25. M. d'Astuto et al., Phys. Rev. Lett. **88**, 167002 (2002).
26. M. Braden et al., Phys. Rev. B **72**, 184517 (2005).
27. The empirical mode-coupling constant λ is estimated by $\lambda = v_{bare}/v_F - 1$ where v_{bare} represents the slope of the straight line connecting the two points in the dispersion at -0.2 eV and E_F and v_F the slope of the measured dispersion between -0.05 eV and E_F.
28. T. Yoshida et al., Phys. Rev. Lett. **91**, 27001 (2003).
29. X. J. Zhou et al., Phys. Rev. Lett. **92**, 187001 (2004).
30. K. M. Shen et al., Science **307**, 901 (2005).
31. N.P. Armitage et al., Phys. Rev. Lett. **86**, 1126 (2001).